Formation of amorphous Ti-50 at.% Pt by solid-state reactions during mechanical alloying

by M.L. Mahlatji*†, S. Chikosha*, H.K. Chikwanda*, W.E. Stumpf†, and C.W. Siyasiya†

Synopsis

Mechanical alloying of an equiatomic mixture of crystalline Ti and Pt elemental powders in a high-energy ball mill formed an amorphous alloy by solid-state reactions. Mechanical alloying was carried out in an argon atmosphere at a rotation speed of 1200 r/min and a 20:1 ball-to-powder weight ratio, for time intervals of 4 to 40 hours. At an intermediate stage of mechanical alloying, scanning electron microscopy showed the formation of characteristic layered structures of inhomogeneous composition within the powder particles. X-ray diffraction analysis showed the gradual disappearance of crystalline Bragg peaks and the emergence of broad amorphous maxima as milling progressed. The amorphization process was completed after 8–12 hours. The amorphous state of the product indicated that temperatures during processing did not exceed the crystallization temperature of the alloy.

Keywords

TiPt alloy, mechanical alloying, amorphization, solid-state reactions.

Introduction

Shape memory alloys (SMAs) undergo a reversible martensite transformation, which drives the thermoelastic properties of shape memory and pseudoelasticity (Otsuka and Ren, 1999). The Ti-50 at.% Pt alloy, which transforms on cooling from the high-temperature cubic B2 phase to the low-temperature orthorhombic B19 phase (Donkersloot and Van Vucht, 1970), has potential for high-temperature shape memory applications. The alloy has a reported martensite transformation temperature (M_S) of 1050°C (Biggs *et al.*, 2001). The pseudoelasticity and shape memory properties of the Ti-50 at.% Pt alloy under stress-free conditions have been well documented (Yamabe-Mitarai *et al.*, 2006, 2010). Shape memory applications in high-temperature environments such as in the aerospace, energy, and automotive industries require alloys with a high M_S range (300-1000°C), much higher than the M_S range reported for the commercially successful Ti-Ni alloys of just over 100°C (Otsuka and Ren, 2005). While the addition of certain alloying elements can slightly raise the M_S of Ti-Ni alloys (Firstov *et al.*, 2004),

higher transformation temperatures can be achieved only by systems with high M_S such as Ti-Pt. Alloying elements can then be used to reduce the M_S according to specific applications and to improve ductility. Reducing the M_S also lowers the effect of diffusion-controlled processes such as recrystallization, recovery, and phase separation, all of which are known to be detrimental to the reversible martensite transformation.

Conventional methods of forming the TiPt alloy usually involve plasma arc, electron beam, or vacuum induction melting, followed by a suitable thermomechanical treatment to homogenize and age the alloy. The current work explores mechanical alloying (MA) as an alternative means of producing the alloy. MA is a process of alloy formation from a mixture of powder particles in a high-energy ball mill (Soni, 2001). Chemical homogenization proceeds through a series of ball-powder-ball collisions (Figure 1), resulting in the repeated flattening, fracturing, and mutual cold welding of the powder particles coupled with short-range diffusion. This leads to the formation of a particulate alloy material suitable for consolidation and further processing.

MA of crystalline powder mixtures of two transition metals often results in the formation of amorphous alloys (Koch *et al.*, 1983; Schwarz and Koch, 1986). It is generally accepted that this is due to solid-state amorphization reactions (SSARs), driven by (a) a large negative heat of mixing in the amorphous state, and (b) one element in the powder mixture having anomalously fast diffusivity in the other (Johnson, 1986). These conditions ensure the availability of a sufficient thermodynamic driving force for the amorphization reaction, and that the

Formation of amorphous Ti-50 at.% Pt by solid-state reactions during mechanical alloying
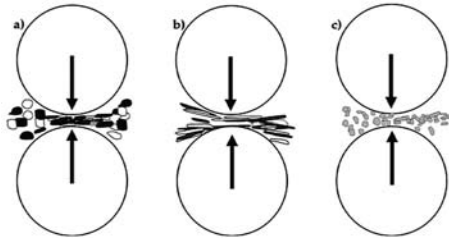

Figure 1—Schematic of the different stages during MA of a nominally ductile powder mixture: a) starting powder; b) flattened, layered composite particles; c) homogenous equiaxed particles

amorphous phase forms at a reasonable rate, faster than the competing crystalline equilibrium phase(s). The free energy state of such a process can be generally illustrated by the schematic free energy diagram (Figure 2), where it is assumed that a fully homogenous amorphous alloy with composition X is formed from a starting crystalline powder mixture of A and B. The free energy of the amorphous phase, indicated by the thick solid curve, is shown together with the dashed schematic free energies of the crystalline α-A(B) and β-B(A) solid solution phases and the equilibrium crystalline γ-intermetallic phase.

The amorphous MA product formed by SSAR is a metastable phase that requires devitrification to form an equilibrium crystalline phase suitable for the envisaged shape memory applications. As Figure 2 suggests, such alloys typically have no thermodynamic barrier against crystal-lization of the amorphous phase, only a kinetic barrier that suppresses the long-range atomic diffusion required for crystallization (Johnson, 1986). The amorphous phase will therefore readily undergo crystallization when heated above the crystallization temperature (T_x), where enough activation energy becomes available to overcome the kinetic barrier against crystallization.

Compared to conventional melting methods, MA offers the advantages of solid-state processing and better composition control, with the possibility of directly forming near net shape parts that require minimum machining and metal loss to produce the final part dimensions. The disadvantages of MA include easy oxidation of powder particles due to the large activated surface area involved, and the formation of a nanocrystalline parent austenite phase. Grain refinement is known to suppress the martensite transformation (Waitz et al., 2004; Guimaraes, 20007). This is due to the increasing difficulty of accommodating the martensite transformation shape strain in the nanocrystalline austenite parent phase. This effect has been demonstrated for Ti-Ni based SMAs formed by crystallization of an amorphous phase (Tian et al., 2009; Valeanu et al., 2011). In the Ti-Pt system, however, Ti-50 at.% Pt has an M_S that lies above the T_x of 477°C (De Reus and Saris, 1990). For such alloys, the amorphous phase can be directly crystallized into the martensite phase with no prior austenite phase, as demonstrated for the Zr-Cu-Ni system (Firstov et al., 2006). The possibility of directly crystallizing B19-TiPt martensite from an amorphous phase removes the limitations that would otherwise be associated with martensite formation from a nanocrystalline B2-austenite parent phase.

Experimental methods

Mechanical alloying

Elemental powders of commercially pure Ti and Pt were mixed in a 1:1 atomic ratio. The Ti particles were spherical and the Pt particles were spongy and irregular (Figure 3). MA was carried out in a Simoloyer CM01® ½ ℓ high-energy horizontal ball mill. The charge, composed of powder and milling balls, was loaded into the jar and the jar was sealed in an Ar-filled glove box. The MA parameters are shown in Table I. The jar was periodically discharged to minimize the cold welding of powder to the milling equipment. The steady state external temperature of the jar did not exceed 37.8°C during MA due to cooling water running through the double-walled jar and flange connection. Cooling the jar increases the transfer of heat away from the contents, promoting brittle particle fracture over ductile coating of the jar walls, balls, and rotor.

Energy-dispersive X-ray analysis (EDX) showed increasing levels of contamination in the powder with increasing MA time. The major contaminants were Fe, Cr, and
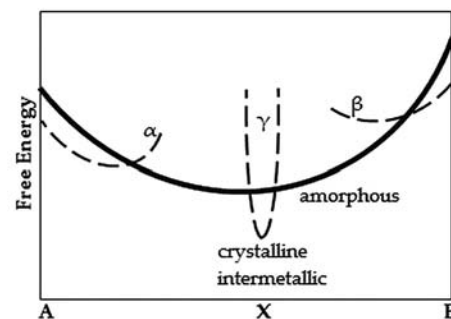

Figure 2—Schematic free energy diagram showing the free energies of the amorphous phase, the crystalline solid solutions α and β, and the crystalline intermetallic γ phase
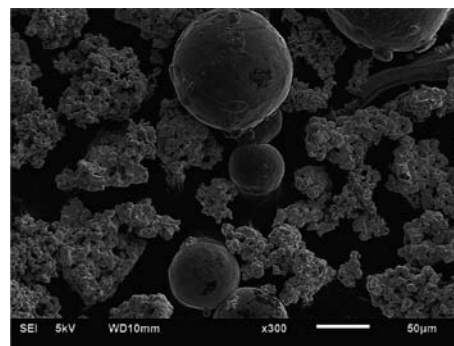

Figure 3—SE-SEM micrograph of the starting powder for MA showing spherical particles (Ti) and spongy, irregular particles (Pt)

Table I

Mechanical alloying parameters

Mill type	Simoloyer CM01® ½
Ball-Powder ratio	20:1 (w/w); 100Cr6 Ø5mm milling balls
Milling intervals	0, 4,8,12,16, 24, 32, 40 hrs
Milling atmosphere	Argon
Milling speed	1200 r/min, operating and discharging runs

Formation of amorphous Ti-50 at.% Pt by solid-state reactions during mechanical alloying

Mo, corresponding to the hardened steel composition of the mill lining and rotor. Hence the contamination was attributed to wear of milling equipment. Fe levels in the milled powder ranged from ≤1 wt% Fe after 4 hours to well over 20 wt% Fe in powder milled for16 hours and longer.

Structural characterization

Phase characterization of the powder was performed using X-ray powder diffraction (XRD) in a Phillips PW 1710® powder diffractometer with Cu Kα radiation ($\lambda = 1.5421$ Å) over the 2θ range of 20–120°. Where applicable, the resulting diffraction patterns were analysed for average domain size and internal strain using the Scherrer method (Suryanarayana and Norton, 1998). Scanning electron microscopy (SEM) was carried out with a JEOL JSM-6510® microscope operating at 20 kV and equipped with an EDX detector. Transmission electron microscopy (TEM) work was performed with a JEOL JSM-2100® microscope operating at 200 kV with a beam current of approximately 112 µA.

Results

Morphology of powder

During the first few hours of MA, the powder displayed a strong tendency to cold weld to the balls and walls of the milling jar due to the ductility of the powder. The cold-welded powder was restricted mostly to a specific region of the jar and could be easily dislodged by turning the jar by 180° at regular intervals and running a discharging procedure. While the formation of a thin coating on milling equipment can help prevent excessive wear and minimize powder contamination, the authors have previously observed that not dislodging the welded particles regularly to reintroduce the powder back into the MA process as free-flowing powder will result in a heterogeneous final product. As MA progressed, plastic deformation strongly reduced the ductility of the powder particles, until cold welding to the milling equipment was no longer observed. Figure 4 shows that for powder milled for 4 and 8 hours, the powder particles transformed from spherical/spongy morphology (Figure 3) to a fissured morphology with a wide particle size distribution.

SEM micrographs of sectioned particles at different stages of the alloying process after MA for 4 hours are shown in Figure 5. EDX analysis showed that the dark grey regions are pure Ti and the lighter grey regions have a composition of 39-51 at.% Pt, while the white regions are Pt-rich. The repeated impact experienced by the powder particles when trapped between colliding balls causes plastic deformations and flattening. Mutual cold welding of these flattened particles result in the lamellar structure of Figure 5(a). A similar layered structure at an intermediate stage of alloying of ductile metal powders was also reported by Benjamin and Volin (1974). The repeated fragmentation and cold welding of the powder particles refined the lamellar structure, resulting in a random orientation of the lamellae within the particles as seen in Figure 5(b). Continued structural refinement resulted in homogenization and disappearance of the layered structure, with the Pt-rich layers in Figure 5(c) being the last to disappear. Beyond 4 hours of MA, all particles displayed a homogenous structure similar to Figure 5(d) with a near equiatomic composition.

Crystallinity of powder

Figure 6 shows a series of selected XRD patterns of Ti-50 at.% Pt powders at different MA time intervals. The pattern at zero hours is a superposition of hcp Ti and fcc Pt reflection peaks, showing that the starting material was a mixture of elemental crystalline powders of Ti and Pt. After 4 hours, all Ti reflection peaks have disappeared and only broad low-
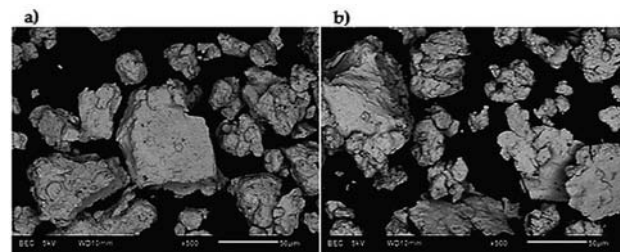

Figure 4—SE-SEM micrographs of Ti-50at%Pt powder particles after MA for (a) 4 and (b) 8 hours
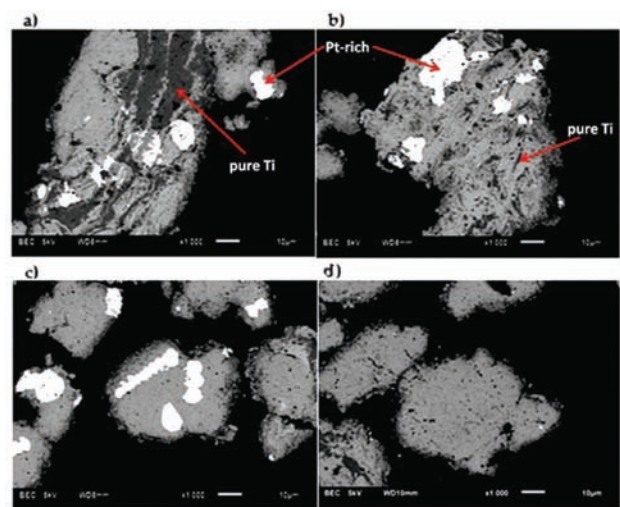

Figure 5—Ti-50at.%Pt cut and polished MA powder particles after 4 hours: (a) lamellar structure with Pt-rich (white) and pure Ti regions (dark grey); (b) randomly oriented lamellae; (c) residual Pt-rich regions in homogenous matrix; (d) complete homogenization
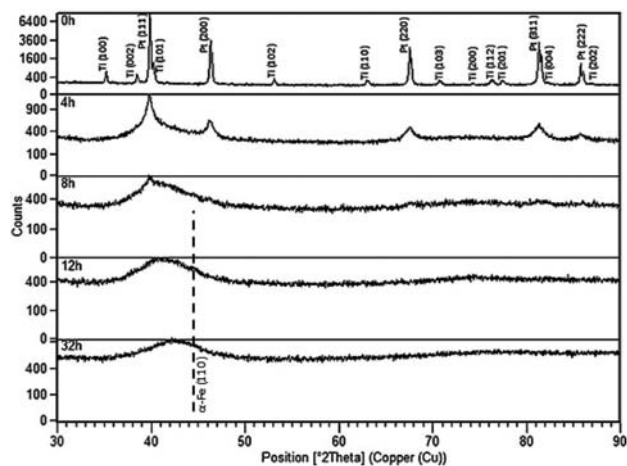

Figure 6—X-Ray diffraction patterns of Ti-50at.%Pt at different MA time intervals, the dotted line shows the position of the α-Fe (110) peak

intensity Pt reflections can be identified. At the same time, there is an emergence of the broad maxima characteristic of amorphous alloys. The Ti layers in the composite layered particles of Figure 5 (a, b) are thinner than 5 μm and were not detected by XRD. Hence, no Ti reflections appear on the 4-hour scans.

The crystallite size of the powder was determined using the Scherrer method (Equation [1]), where d is the average domain dimension along the scattering vector (Å), K is a shape constant (= 0.9), λ is the wavelength ($K\alpha_{Cu}= \lambda$ = 1.5421 Å), θ is the X-ray scattering angle, and β is the line width (FWHM) after correction for instrument broadening with a Si standard. The tangent formula in Equation [2] was used to determine the internal strain, where ε is the mean lattice distortion, and β and θ are the same as for Equation [1]. The average crystallite size is reduced (and the lattice strain is increased) from 13 nm (0.87%) after 4 hours to 8.3 nm (1.30%) after 8 hours. For MA of 12 hours and beyond, all Bragg reflections had disappeared, indicating completion of the amorphization process.

$$d = \frac{K\lambda}{\beta \cos\theta} \qquad [1]$$

$$\varepsilon = \frac{\beta}{4 \tan\theta} \qquad [2]$$

The accumulation of crystalline contaminants (mostly Fe) from wear of milling equipment as detected by EDX is not immediately apparent in the XRD patterns of Figure 6 due to the low resolution of XRD. The fully amorphous reflection after 12 hours, where the contamination level was still relatively low, has the major maximum centred near the 2θ position corresponding to the strong fcc Pt (111) and hcp Ti (101) Bragg reflections, as expected. The 32-hour pattern, however, shows how the major maximum had gradually shifted and is now centred at a higher 2θ position, due to the accumulation of Fe-rich contaminants (the highest intensity peak of bcc α-Fe (110) is $2\theta= 44.674°$).

The MA process was further studied by TEM for the time intervals corresponding to partial amorphization (4 hours' MA), fully amorphous alloy (12 hours), and heavily contaminated amorphous alloy (32 hours). Figure 7 (a, b) shows TEM images with corresponding selected area diffraction (SAD) patterns after MA for 4 hours, where the amorphous phase co-exists with un-reacted Ti and Pt. This is reflected by the fine lattice fringes on the high-magnification image (arrow) and diffraction spots on the SAD. The lack of diffraction spots and lattice fringes on the powder after 12 hours (Figure 8a and b) shows that the powder is now fully amorphous, in agreement with the XRD results. After 32 hours (Figure 9a and b), SAD patterns show traces of crystalline diffraction spots in the amorphous matrix. The crystalline spots can be due to either: (a) crystallization of the previously fully amorphous powder when the powder particles trapped between colliding balls experience a momentary temperature rise exceeding the T_x of the alloy (as Figure 2 suggests), or (b) the introduction of crystalline contaminant phases into the amorphous alloy. The temperature rise from ball impacts during MA has been estimated to be only a few hundred degrees (Joarder *et al.*, 2004), well below the reported T_x of amorphous Ti-50 at.% Pt alloy. The crystallites can therefore be attributed to contam-

inants from wear of milling equipment, as detected by the low-resolution analytical techniques. This indicates that to avoid contamination, MA should not be carried out for unnecessarily long time intervals, such as beyond the point of complete amorphization.

Discussion

The formation of amorphous Ti-50 at.% Pt alloy is demonstrated by the transformation of Bragg elemental Ti and Pt crystalline reflections at the start of MA into broad, featureless reflections characteristic of amorphous alloys after 8–12 hours of MA. Similar results of amorphous phase formation by MA from elemental powder mixtures have been reported for the closely related TiNi (Schwarz *et al.*, 1985;
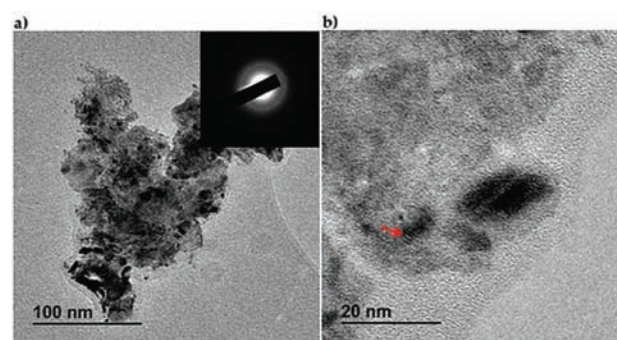

Figure 7—Ti-50at.%Pt powder after MA for 4 hours: (a) The SAD pattern shows an amorphous halo and crystalline diffraction spots, corresponding to the remaining crystalline phases; (b) lattice fringes (arrow) in an amorphous matrix
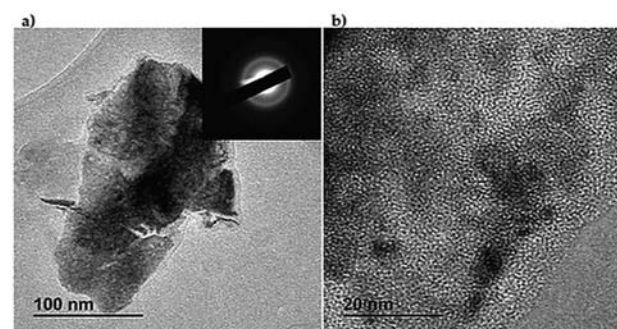

Figure 8—Ti-50at.%Pt powder after MA for 12 hours: (a) TEM image with corresponding SAD pattern showing the amorphous halo, (b) the amorphous phase
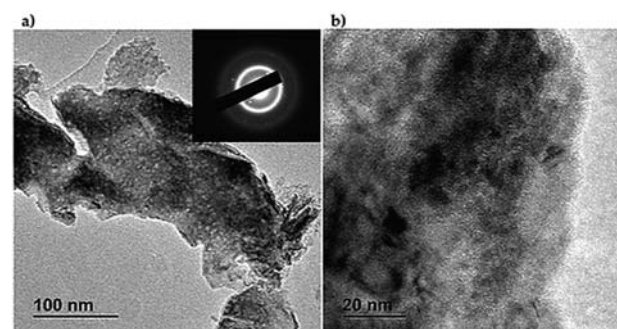

Figure 9—Ti-50at.%Pt powder after MA of 32 hours: (a) The SAD pattern shows the amorphous halo and crystalline diffraction spots, attributed to contamination from wear of milling equipment; (b) the amorphous phase

Formation of amorphous Ti-50 at.% Pt by solid-state reactions during mechanical alloying

Liang et al., 1995) and TiPd (Thompson and Politis, 1987) systems. The deformation, fracturing, and cold welding of powder particles is illustrated by Figure 4 (a, b), where the formerly spherical and spongy particles had formed agglomerates, and in some cases had become flattened and fissured. These structural changes also resulted in a reduction in crystallite size and an increase in lattice strain. The characteristic layered structure shown in Figure 5, which precedes the appearance of the homogenous structure, indicates that the alloying process proceeded by SSAR. The layered structure was due to the preferential cold welding of newly created clean Ti and Pt boundaries formed by particle fracture. It has been suggested that conditions at the layer interfaces during an intermediate stage of MA of two metals closely resemble those within conventional thin-film diffusion couples (Johnson, 1988), leading to alloy formation by solid-state interfacial interdiffusion reactions. According to the classification of Weeber and Bakker (1988), SSAR of two metals can proceed along three different paths, depending on the alloy system and experimental conditions. The XRD patterns of Figure 6 indicate that the Ti-50 at.% Pt alloy underwent a Type II reaction path, characterized by a decrement in intensity of the elemental crystalline reflections and an increment in intensity of the broad amorphous reflection.

The SSAR alloying mechanism observed in the current work is different from the observation made by Maweja et. al., (2012), where MA of Ti-50 at.% Pt powder in a high-energy ball resulted in formation of a disordered crystalline fcc Pt(Ti) extended solid solution. It is suggested that the different MA product phases were due to differences in milling parameters, such as the effect of using a process control agent (PCA) to control the cold welding of powder particles to milling equipment. A PCA was not used in the current work to avoid contamination and to optimize alloy formation. Besides improving the amount of free-flowing powder in the milling jar, PCAs have been shown to have a generally negative effect on the alloying process (Machio et al., 2011). Similar inconsistencies in the crystallinity of the milled product have been observed in the MA of other alloy systems such as Ti-Ni, where formation of solid solutions (Mousavi et al., 2008) and disordered intermetallics (Takasaki, 1998) have been reported in addition to amorphous phase formation when using different MA parameters. Determination of the relative thermodynamic stability of the fcc Pt(Ti) solid solution (reported by Maweja et. al., 2012), the amorphous phase (reported in the current work), and the crystalline equilibrium phase under conditions of suppressed atomic diffusion (illustrated in Figure 2) is required for a better understanding of phase transformations during MA of the Ti-Pt system.

While it is currently possible to measure the process temperature during operation of the high-energy ball mill only with a thermocouple attached externally to the wall of the milling jar, some general deductions can be made about thermal conditions inside the jar during operation. Two temperatures can be defined: (a) the ambient temperature in the jar, and (b) the momentary temperature rise during high-speed ball collisions, which is expected to be much higher than the ambient temperature. The amorphous phase is expected to readily crystallize into an equilibrium crystalline phase when heated above the T_x of the alloy. The fully amorphous state of the milled powder after 8–12 hours shows that both the ambient and the ball-collision temperatures inside the milling jar did not exceed the T_x of the alloy, otherwise the alloy powder would have become crystalline.

Conclusions

i. Amorphous Ti-50 at.% Pt alloy was formed by SSAR during MA of crystalline elemental powders of Ti and Pt. At an intermediate stage, the mechanical mixing and deformation led to formation of characteristic layered particles. Amorphization was completed after 8–12 hours. Milling for longer time intervals beyond the completion of amorphization should be avoided as it would result in powder contamination from wear of milling equipment. While it was possible to measure only the external temperature of the milling jar, it can be inferred from the amorphous state of the product that the temperature during processing did not exceed the T_x of the alloy

ii. Analogies can be drawn between the formation of a homogenous amorphous alloy by MA and the formation of a homogenous molten alloy by ordinary melting. A liquid and an amorphous alloy with the same composition represent the 'molten'and 'frozen' intermediate states in the process of forming crystalline alloys. The former requires cooling towards T_x and the latter requires heating towards T_x to form the equilibrium crystalline phase. An amorphous Ti-50 at.% Pt alloy formed by MA therefore represents a 'molten' phase, formed without heating above the extremely high melting points of the components and of the intermetallic phase

iii. Future work includes devitrification of the amorphous alloy to form crystalline Ti-50 at.% Pt suitable for shape memory testing. Semi-empirical thermodynamic modelling will be done to establish solid solubility limits of Ti in fcc Pt under polymorphic conditions, as well as the relative free energies of the solid solution and the amorphous and the crystalline α-TiPt phases at temperature below the T_x. This is required to understand the differences in the product phases formed during MA of the Ti-Pt system.

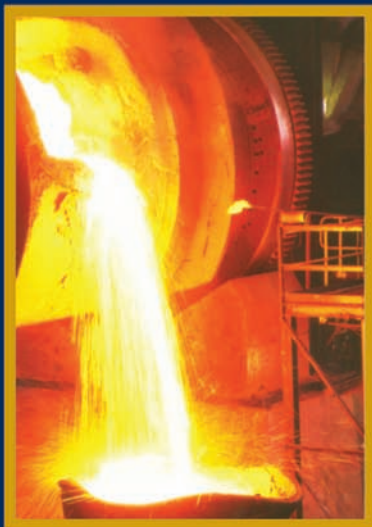## References

BENJAMIN, J.S. and VOLIN, T.E. 1974. The mechanism of mechanical alloying. *Metallurgical Transactions*, vol. 5. pp.1929-1934.

BIGGS, T., CORTIE, M.B., WITCOMB, M.J., and CORNISH, L.A. 2001. Martensitic transformations, microstructure, and mechanical workability of TiPt. *Metallurgical and Materials Transactions A*, vol. 32A. pp. 1881–1886.

DE REUS, R. and SARIS, F.W. 1990. The crystallization temperature of amorphous transition-metal alloys. *Materials Letters*, vol. 9, no. 12. pp. 487–493.

DONKERSLOOT, H.C. and VAN VUCHT, J.H.N. 1970. Martensitic transformations in gold-titanium, palladium-titanium and platinum-titanium alloys near the equiatomic composition. *Journal of the Less-Common Metals*, vol. 20. pp. 83–91.

Formation of amorphous Ti-50 at.% Pt by solid-state reactions during mechanical alloying

FIRSTOV, G.S., VAN HUMBEECK, J., and KOVAL, Y.N. 2004. High-temperature shape memory alloys: some recent developments. *Materials Science and Engineering A*, vol. A378. pp. 2–10.

FIRSTOV, G.S., KOVAL, Y.N., VAN HUMBEECK, J., PORTIER, R., VERMAUT, P., and OCHIN, P. 2006. Phase transformations in Zr-29.56at.%Cu-19.85at.%Ni melt-spun high-temperature shape memory alloy. *Materials Science and Engineering A*, vol. A438–440. pp. 816–820.

GUIMARÃES, J.R.C. 2007. Excess driving force to initiate martensite transformation in fine-grained austenite. *ScriptaMaterialia*, vol. 57. pp. 237–239.

JOARDAR, J., PABI, S.K., and MURTY, B.S. 2004. Estimation of entrapped powder temperature during mechanical alloying. *Scripta Materialia*, vol. 50. pp. 1199–1202.

JOHNSON, W.L. 1986. Thermodynamic and kinetic aspects of the crystal to glass transformation in metallic materials. *Progress in Materials Science*, vol. 30. pp. 81–134.

JOHNSON, W.L. 1988. Crystal-to-glass transformation in metallic materials. *Materials Science and Engineering*, vol. 97. pp. 1–13.

KOCH, C.C., CAVIN, O.B., MCKAMEY, C.G., and SCARBROUGH, J.O. 1983. Preparation of 'amorphous' Ni60Nb40 by mechanical alloying. *Applied Physics Letters*. vol. 43. pp. 1017–1019.

LIANG, G.X., WANG, E.D., and LI, Z.M. 1995. Effects of ball milling intensity on structural changes in mixed 50Ni-50Ti powders during mechanical alloying process. *Materials Science and Technology*, vol. 11. pp. 347–350.

MACHIO, C., CHIKWANDA, H., and CHIKOSHA, S. 2011. Effect of process control agent (PCA) on the characteristics of mechanically alloyed Ti-Mg powders. *Journal of the Southern African Institute of Mining and Metallurgy*, vol. 111. pp. 149–153.

MAWEJA, K., PHASHA, M.J., and YAMABE-MITARAI, Y. 2012. Alloying and microstructural changes in platinum-titanium and annealed powders. *Journal of Alloys and Compounds*, vol. 523. pp. 167–175.

MOUSAVI, T., KARIMZADEH, F., and ABBASI, M.H. 2008. Synthesis and characterization of nanocrystalline NiTi intermetallic by mechanical alloying. *Materials Science and Engineering A*, vol. 487. pp. 46–51.

OTSUKA, K. and REN, X. 1999. Recent developments in the research of shape memory alloys. *Intermetallics*, vol. 7. pp. 511–528.

OTSUKA, K. and REN, X. 2005. Physical metallurgy of Ti-Ni-based shape memory alloys. *Progress in Materials Science*, vol. 50. pp. 511–687.

SCHWARZ, R.B., PETRICH, R.R., and SAW, C.K. 1985. The synthesis of amorphous Ni-Ti alloy powders by mechanical alloying. *Journal of Non-Crystalline Solids*, vol. 76. pp. 281–302.

SCHWARZ, R.B., and KOCH, C.C. 1986. Formation of amorphous alloys by the mechanical alloying of crystalline powders of pure metals and powders of intermetallics. *Applied Physics Letters*, vol. 49. pp. 146–148.

SONI, P.R. 2001. Mechanical Alloying: Fundamentals and Applications. Cambridge International Science Publishing, Cambridge.

SURYANARAYANA, C. and NORTON, M.G. 1998. X-Ray Diffraction. A Practical Approach. Plenum Press, New York.

TAKASAKI, A. 1998. Mechanical alloying of the Ti-Ni system. *Physica Status Solidi (a)*, vol. 169. pp.183–191.

THOMPSON, J.R. and POLITIS, C. 1987. Formation of amorphous Ti-Pd alloys by mechanical alloying methods. *Europhysics Letters*, vol. 3. pp. 199–205.

TIAN, B., TONG, Y.X., CHEN, F., LIU, Y., and ZHENG, Y.F. 2009. Phase transformation of NiTi shape memory alloy powders prepared by ball milling. *Journal of Alloys and Compounds*, vol. 477. pp. 576–579.

VALEANU, M., LUCACI, M., CRISANO, A.D., SOFRONIE, M., LEONAT, L., and KUNCSER, V. 2011. Martensitic transformation if Ti50Ni30Cu20 alloy prepared by powder metallurgy. *Journal of Alloys and Compounds*, vol. 509. pp. 4495–4498.

WAITZ, T., KAZYKHANOV, V., and KARNTHALER, H.P. 2004. Martensitic phase transformations in nanocrystalline NiTi studied by TEM. *Acta Materialia*, vol. 52. pp. 137–147.

WEEBER, A.W. and BAKER, H. 1988. Amorphization by ball milling. A review. *Physica B*, vol. 153. pp. 93–135.

YAMABE-MITARAI, Y., HARA, T., MIURA, S., and HOSODA, H. 2010. Shape memory effect and pseudoelasticity of TiPt. *Intermetallics*, vol. 18. pp. 2275–2280.

YAMABE-MITARAI, Y., HARA, T., MIURA, S., and HOSODA, H. 2006. Mechanical properties of Ti-50(Pt,Ir) high-temperature shape memory alloys. *Materials Transactions*, vol. 47, no. 3. pp. 650–657. ◆